Supporting Information

A Chameleon-like Core-Shell Organic/Lanthanide Flexible Crystal Waveguide for Bandwidth and Colour Tunability

Melchi Chosenyah, Mehdi Rohullah, Avulu Vinod Kumar, K. V. Jovan Jose, and Rajadurai Chandrasekar**

Table of contents

1. Materials

All chemicals and solvents like hexane, dichloromethane, toluene, and 1,4-dioxane were purchased from commercial sources (TCI chemicals, Sigma Aldrich, BLD chemicals, and Merck). Unless specified, HPLC solvents were used for synthesis and self-assembly. Europium(III) thenoyltrifluoroacetonate ($Eu(tta)_3$) hydrate, is purchased from Acros Organics.

2. Synthesis and preparation of BPP microcrystals

a) Synthesis of BPP:

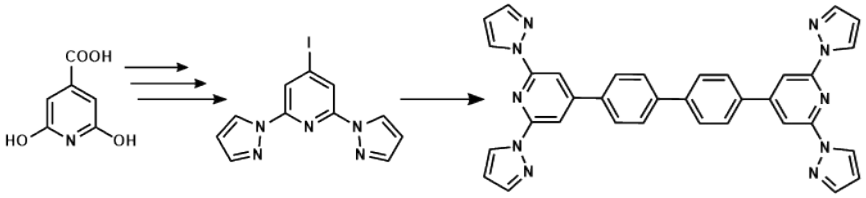

Scheme S1 Synthetic scheme of BPP molecule. (Reaction conditions: 4,4'-biphenylenediboronicacid, $[Pd(PPh_3)_4]$ and 2M Na_2CO_3/1,4-Dioxane/72 hours/70 °C).[1]

b) Preparation of microrods

For self-assembly studies, in a clean vial, BPP (0.2 mg) was dissolved in DCM (1 mL) and left undisturbed at rt for 8 h. This solution under slow evaporation condition formed needle-like crystals. Again 1 mL of DCM was used to dissolve the formed crystals. Drop casting 2-3 drops of this DCM solution of BPP onto a clean glass coverslip produced long microrods after complete evaporation of the solvent.

3. Instrumental methods

a) Solid-state absorption and emission studies: The solid-state absorption measurements were done on Shimadzu UV-3600 spectrometer in a diffuse reflectance UV−visible (DR−UV−vis) mode. The reflectance spectra were converted to an absorbance using the Kubelka−Munk function. The solid-state emission spectra were collected using JASCO FP-8500 spectrofluorometer.

b) Confocal microspectroscopy studies: The optical experiments of a single microcrystal were carried out on a backscattering mode setup of the Wi-Tec alpha 300 AR laser confocal optical microscope (LCOM) equipped with a Peltier-cooled CCD detector. Using 300 grooves/mm grating BLZ = 750 nm, the accumulation time was adjusted to 10, and the integration time was typically made 0.5 s per spectra. 355/405 nm, 532 nm, and 785 nm lasers were used as excitation sources. The output signal collection was performed using 20× (N.A. = 0.6) objective. The signal was sent to a CCD detector through a multimode optical fiber of diameter 100 μm (3 μm core). All measurements were performed at ambient condition and images were processed using WI-TEC

software. The spectra were baseline corrected before analysis. 20x objective was used for spectra and image collection.

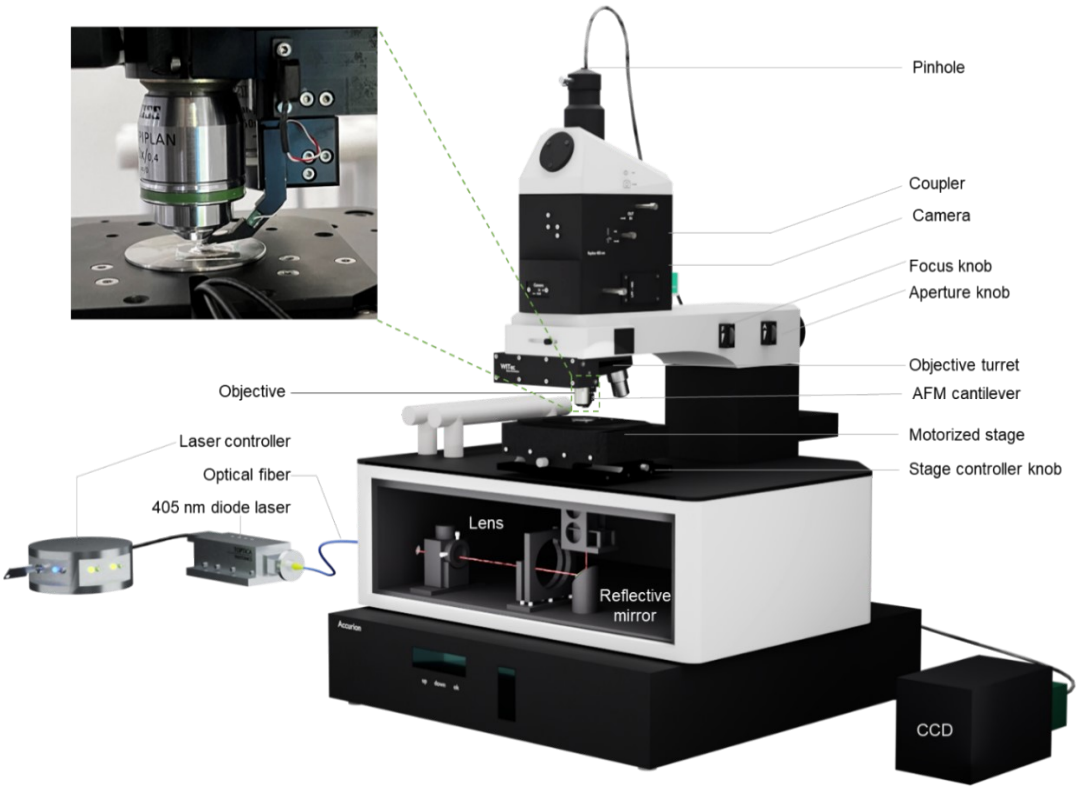

Scheme S2 Graphical illustration of confocal optical microscopy. Inset shows the image of attached AFM cantilever tip for the crystal manipulation.

c) **Micromanipulation of the crystals:** The micromanipulation experiments were performed using an AFM attached to the above-mentioned confocal microscope setup. Using an AFM cantilever, single un-coordinated and coordinated BPP microcrystals were manipulated to attain a bent geometry. An AFM cantilever (Adama: NM-TC, with a force constant of 350 N/m and a typical tip radius of 25 +/- 10 nm) was used for the mechanical manipulation.

d) **Field emission scanning electron (FESEM) microscopy studies:** The morphological analysis and energy dispersive X-ray (EDX) analysis of microrods were performed using a Zeiss field emission scanning electron microscope (FESEM) operating at 3 kV. All the experiments were performed after gold coating before imaging.

e) **Transmission electron microscopy (TEM) studies:** The microstructures were probed for their detailed morphology and crystalline nature using a multi-purpose JEOL F200 transmission electron microscope (TEM) operating at 200 kV accelerating voltage. Selected area electron diffraction (SAED) pattern was analysed using CrystBox software.

f) **Powder X-ray diffraction analysis:** Powder X-ray diffraction pattern of the coordination complex [$Eu(tta)_3$(BPP)] was recorded on Bruker D8 Advance diffractometer (Bruker-AXS,

Karlsruhe, Germany) using Cu-Kα X-radiation (λ = 1.5406 Å) at 40 kV and 30 mA power, over the 2θ range 5–50° at a scan rate of 5°/min.

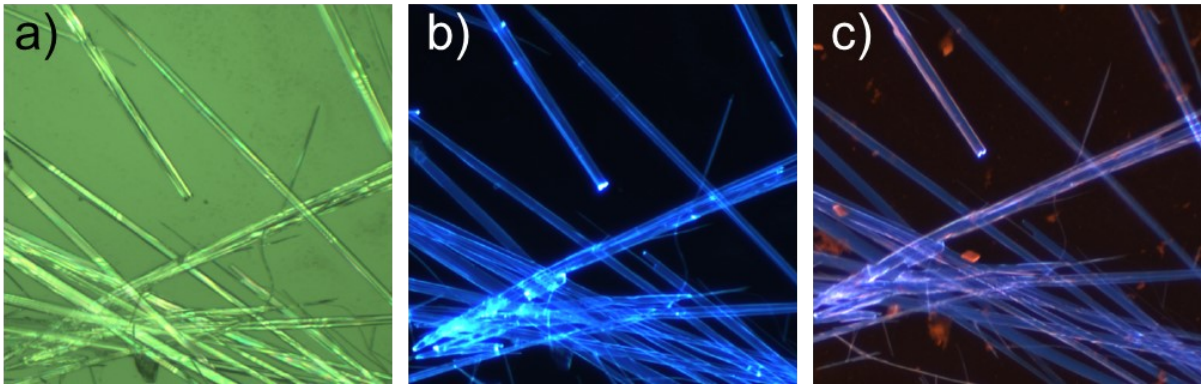

Figure S1 a) Confocal optical image of BPP microcrystals. FL images of b) Un-coordinated and c) Coordinated BPP microcrystals.

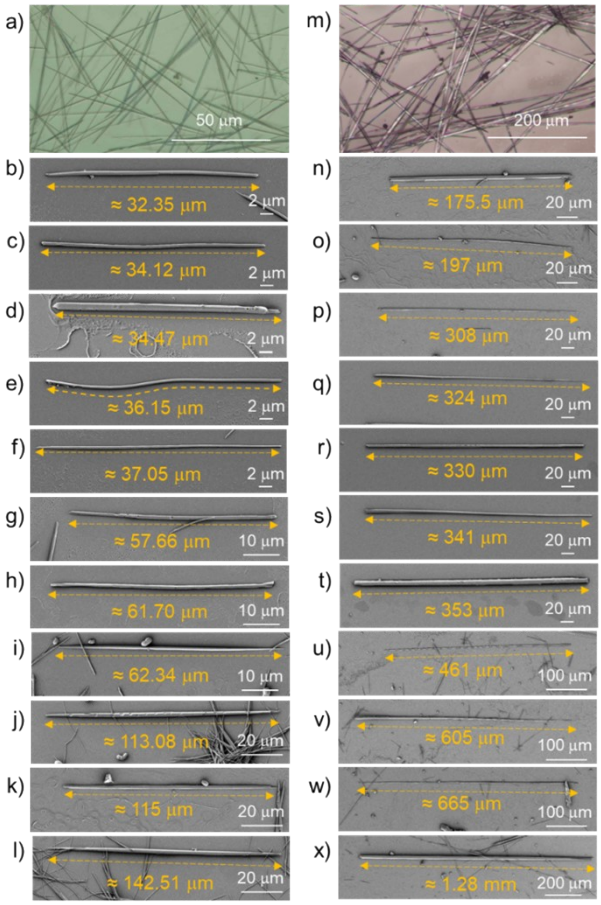

Figure S2 a) Optical and b-l) FESEM images of the BPP microcrystal with the varying length from ≈ 32 µm to ≈ 142 µm. m) Optical and n-x) FESEM images of the BPP microcrystal with the varying length from ≈ 175 µm to ≈ 1.28 mm.

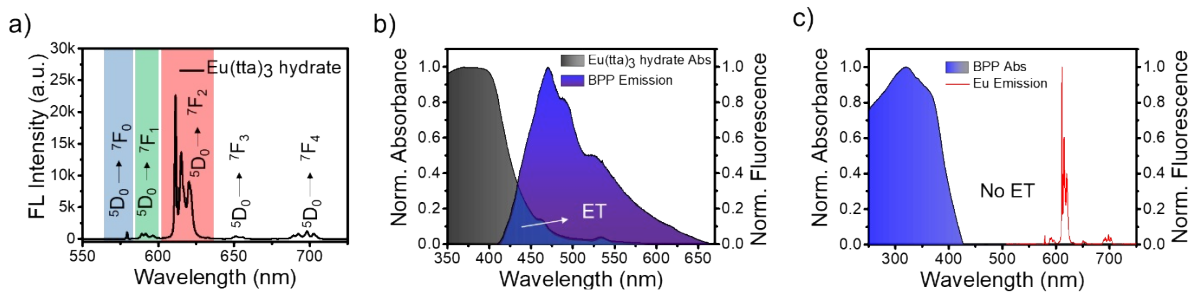

Figure S3 Solid-state optical properties of the BPP and Eu(tta)$_3$ hydrate. a) Hypersensitive narrow band *f-f* transitions of Eu(III) ion. b) Radiative energy transfer from BPP to Eu(III). c) No energy transfer from E(III) to BPP.

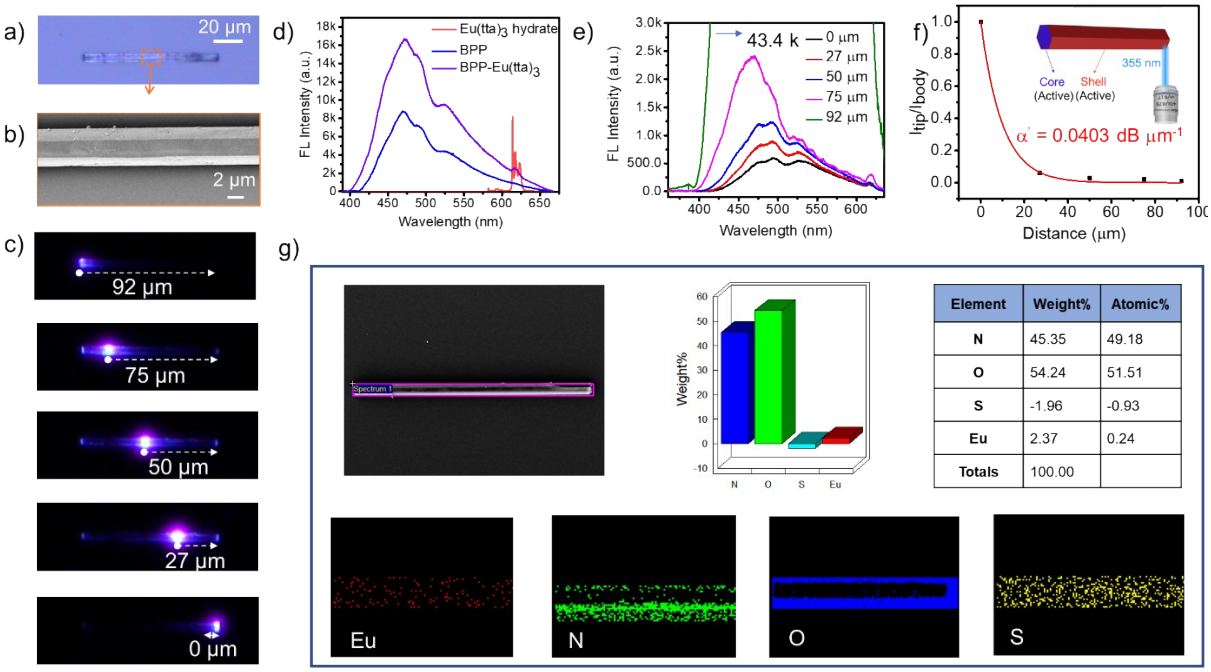

Figure S4 a) Confocal optical image, b) FESEM image, and c) FL images of Eu(tta)$_3$ coordinated BPP microcrystal. d) Spectral comparision of BPP, Eu(tta)$_3$ hydrate, and BPP-Eu(tta)$_3$. e) The excitation position-dependent FL spectra obtained from the BPP-Eu(tta)$_3$. f) Optical loss plot of the BPP-Eu(tta)$_3$. Inset: Graphical representation of the excitation for optical waveguiding. g) FESEM-EDX data collected in a selected area on microrod confirming the presence of Eu element on the surface of the BPP microcrystal.

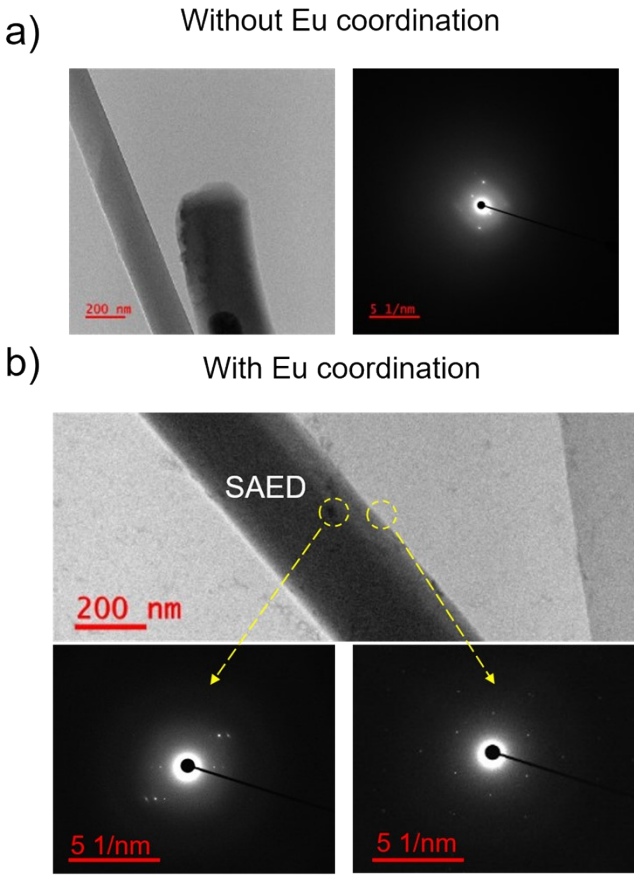

Figure S5 TEM images and selected area diffraction pattern(s) of a) un-coordinated and b) coordinated BPP microcrystals.

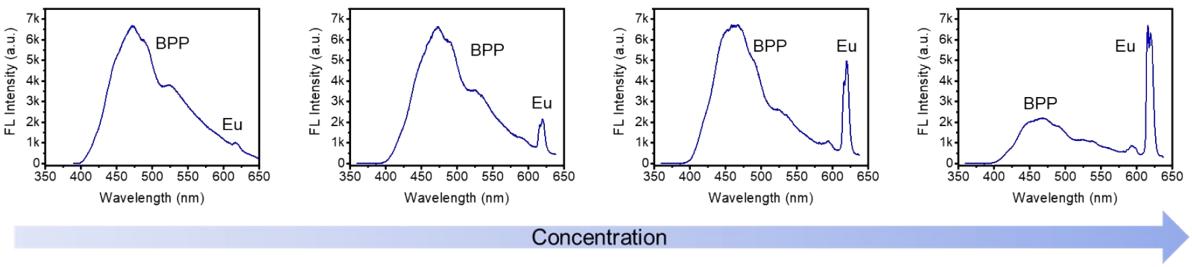

Figure S6 FL spectra of $Eu(tta)_3$ coordinated BPP with varying concentration.

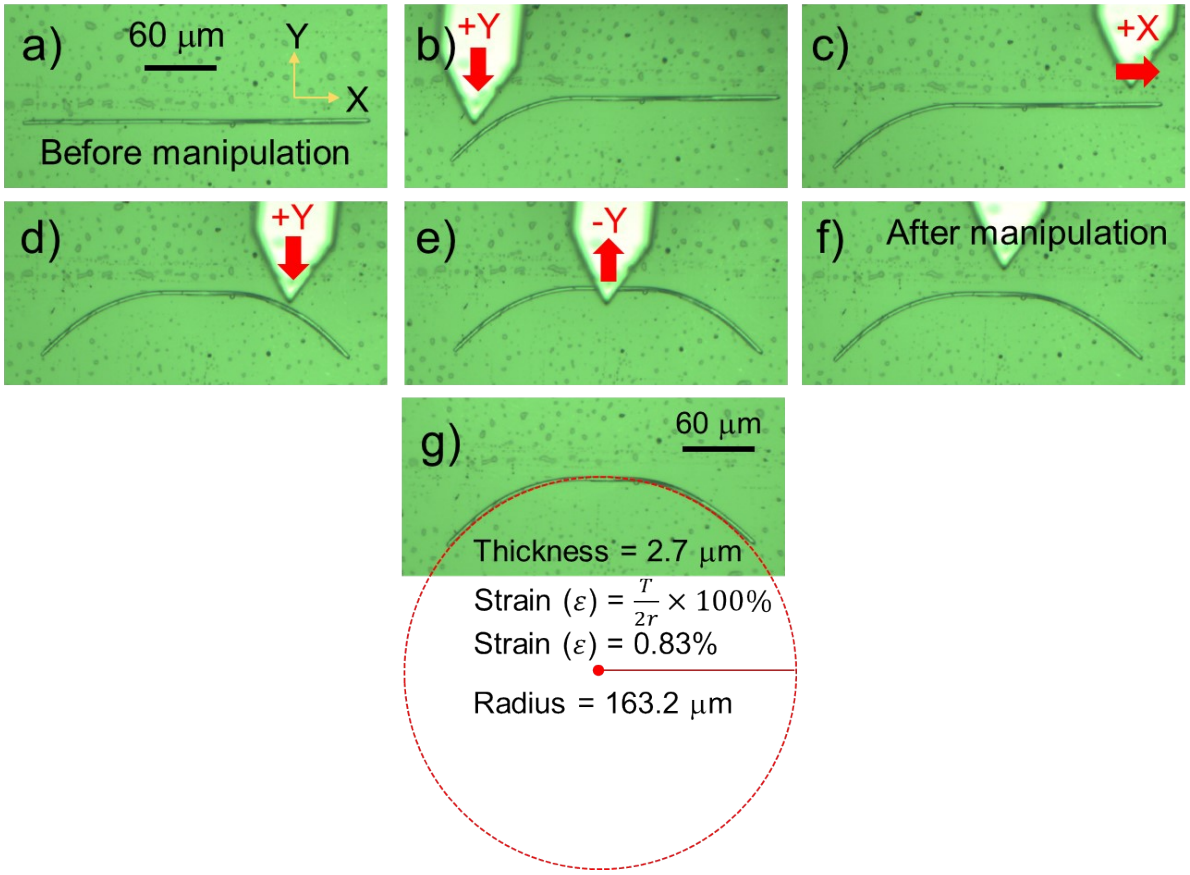

Figure S7 a-g) Micromanipulation of coordinated BPP crystal and strain caused due to bending of straight crystal with AFM tip. g) Strain calculation of the bent region.

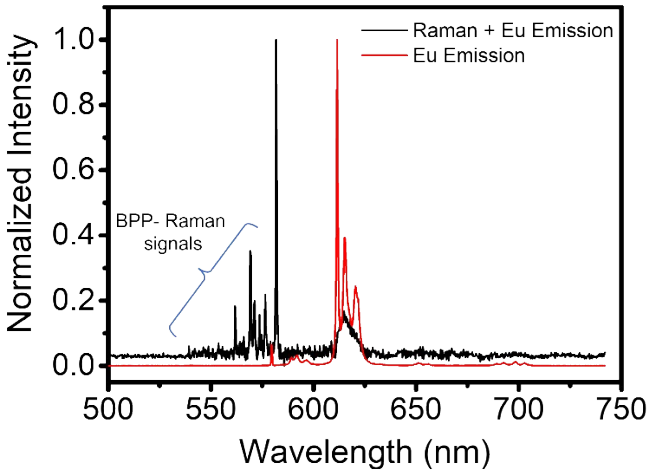

Figure S8 Raman along with FL spectrum collected when excited the $Eu(tta)_3$ coordinated BPP with 532 nm lasers light. FL spectrum of $Eu(tta)_3$ (λ_{ex} = 532 nm) is overlapped with the spectrum obtained from the $Eu(tta)_3$ coordinated BPP.

Table S1 The CIE 1931 diagram's x, y coordinates (colour coordinates) for BPP, $Eu(tta)_3$ hydrate, $Eu(tta)_3$ coordinated BPP when irradiated with 355 nm, 532 nm and 785 nm Lasers.

Emission source	CIE 1931	
	x	y
BPP	0.20261	0.28014
$Eu(tta)_3$ hydrate	0.66668	0.32127
Eu coordinated BPP (λ_{ex} = 355 nm)	0.21097	0.2808
Eu coordinated BPP (λ_{ex} = 532 nm)	0.33627	0.39639
Eu coordinated BPP (λ_{ex} = 785 nm)	0.73234	0.26766

4. Theoretical Raman spectral calculations

The molecular geometry optimization is performed on the ligand (BPP), $Eu(tta)_3$ hydrate, and $Eu(tta)_3$ coordinated BPP complexes at Becke three parameters hybrid functional with Lee–Yang–Parr correlation functional (B3LYP) level of theory with Def2svp basis set, using the Gaussian09 suite of programs.[2] The local minimal characteristics of the optimized geometries of $Eu(tta)_3$ coordinated BPP complex is confirmed by the absence of imaginary normal vibrational modes and optimized structure is depicted in Figure 3a. The Raman spectra of the ligand and coordination complexes are calculated at the same level of theory and basis set on the optimized geometries. Figure 3c depicts the Raman spectra of $Eu(tta)_3$ coordinated BPP complex and a comparison with experimental spectra is presented in the results and discussion session.

5. Synthesis and characterisation of coordination complex [$Eu(tta)_3$(BPP)]

BPP (15 mg, 0.026 mmol) and Europium(III) thenoyltrifluoroacetonate hydrate (46 mg, 0.026 mmol) were dissolved in 20 mL toluene. The reaction mixture was refluxed for 12 h at 110 °C. The solvent was removed under vacuum, leaving a brown solid as a product. Unfortunately, we couldn't obtain the single crystals of coordination complex [$Eu(tta)_3$(BPP)] since the growth of single crystal was hindered by solubility issues and solvent compatibility constraints between the core and shell components, which prevented us from identifying a common solvent system conducive to single-crystal growth.

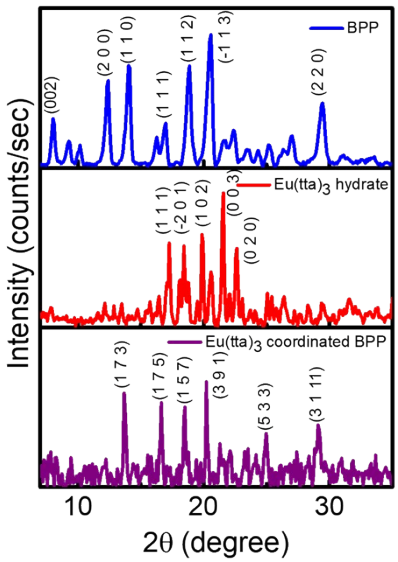

Figure S9 PXRD data of BPP, $Eu(tta)_3$ hydrate, and $Eu(tta)_3$ coordinated BPP. The hkl values are identified using xpert-highscore software.

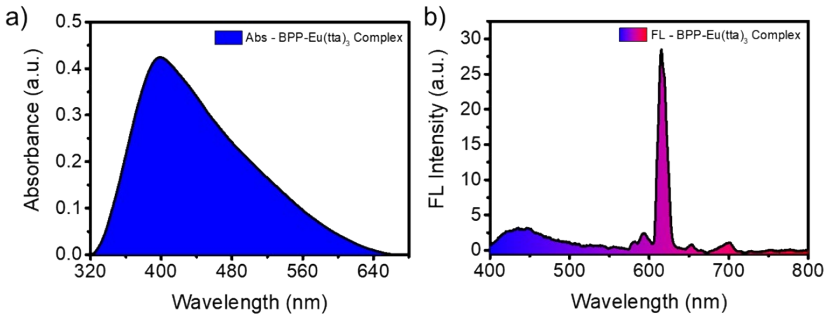

Figure S10 Solid-state a) Absorption and b) Emission spectra of $[Eu(tta)_3(BPP)]$ coordination complex.

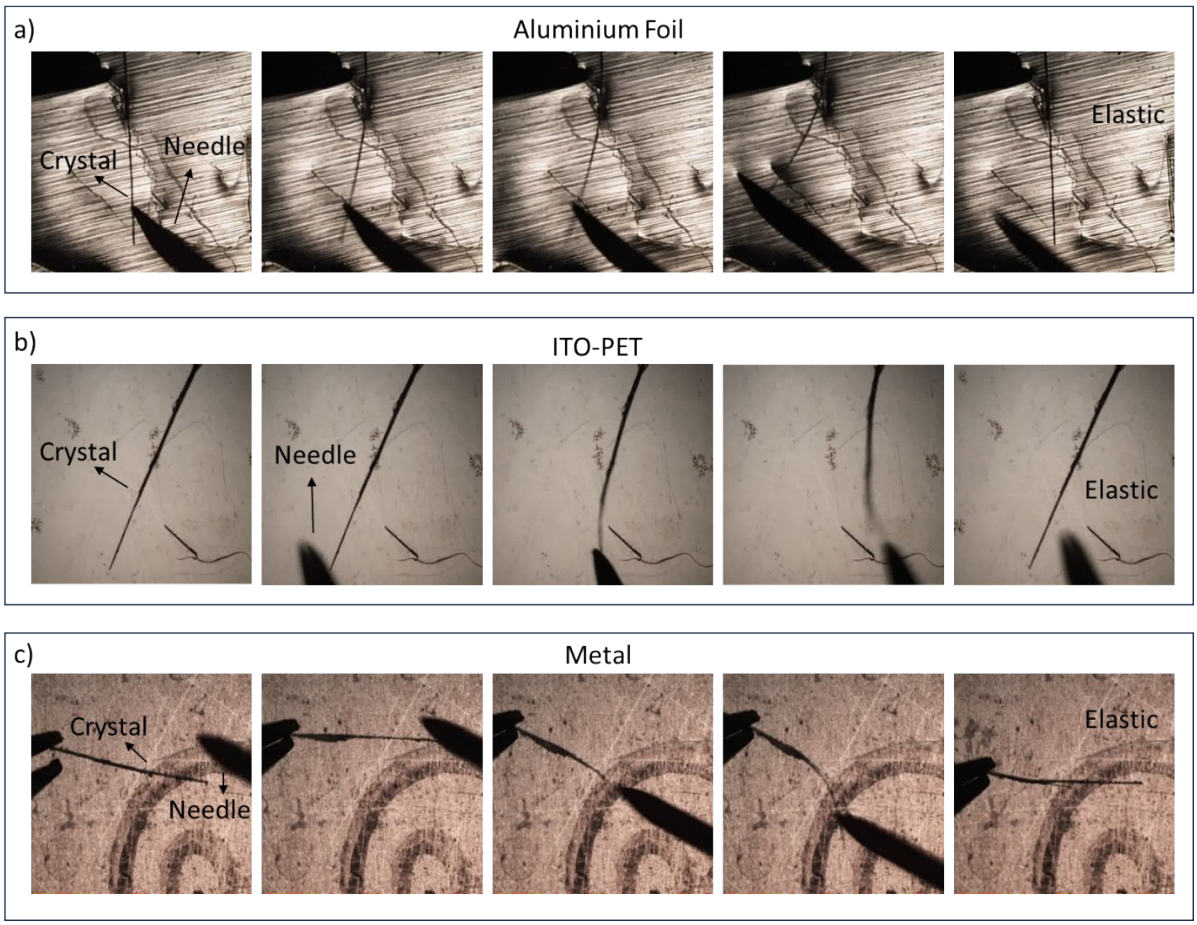

Figure S11 Optical images of the two-point bending test of BPP using tweezers and needles, demonstrating its elastic behavior on different substrates such as aluminium foil, ITO–PET, and a metal sheet, respectively.

6. References

[1] N. Chandrasekhar, R. Chandrasekar, *Chem. Commun.,* 2010, **46**, 2915.

[2] Gaussian 09, Revision C.01, M. J. Frisch, G. W. Trucks, H. B. Schlegel, G. E. Scuseria, M.A. Robb, J. R. Cheeseman, G. Scalmani, V. Barone, B. Mennucci, G. A. Petersson, H.Nakatsuji, M. Caricato, X. Li, H. P. Hratchian, A. F. Izmaylov, J. Bloino, G. Zheng, J. L.Sonnenberg, M. Hada, M. Ehara, K. Toyota, R. Fukuda, J. Hasegawa, M. Ishida, T. Nakajima,Y. Honda, O. Kitao, H. Nakai, T. Vreven, J. A. Montgomery, Jr., J. E. Peralta, F. Ogliaro, M.Bearpark, J. J. Heyd, E. Brothers, K. N. Kudin, V. N. Staroverov, R. Kobayashi, J. Normand,K. Raghavachari, A. Rendell, J. C. Burant, S. S. Iyengar, J. Tomasi, M. Cossi, N. Rega, J. M.Millam, M. Klene, J. E. Knox, J. B. Cross, V. Bakken, C. Adamo, J. Jaramillo, R. Gomperts, R.E. Stratmann, O. Yazyev, A. J. Austin, R. Cammi, C. Pomelli, J. W. Ochterski, R. L. Martin, K.Morokuma, V. G. Zakrzewski, G. A. Voth, P. Salvador, J. J. Dannenberg, S. Dapprich, A. D.Daniels, Ö. Farkas, J. B. Foresman, J. V. Ortiz, J. Cioslowski, and D. J. Fox, Gaussian, Inc.,Wallingford CT, 2009.